BOLETIN DE LA SOCIEDAD ESPAÑOLA DE
Cerámica y Vidrio
www.elsevier.es/bsecv

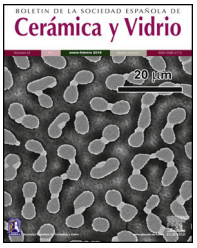

Original

Microstructure, hardness and flexural strength of Ni/Al_2O_3 FGMs by pressure-less sintering with different cooling rates

*K. Ananta Bhaskararao**, *G. Ranga Janardhana*

Department of Mechanical Engineering, University College of Engineering, JNTUK, Kakinada 533003, India

ARTICLE INFO

Article history:
Received 5 November 2019
Accepted 26 March 2020
Available online 18 April 2020

Keywords:
Functionally graded material
Nickel
Alumina
Powder metallurgy
Cooling rate

ABSTRACT

In this work, four-layered functionally graded materials (FGMs) are fabricated with nickel (Ni) and alumina (Al_2O_3) as principle materials. Four FGMs of different compositional layers such as PLS10, PLS15, PLS20 and PLS25 are prepared through powder metallurgy. Developing the Ni/Al_2O_3 FGMs starts with weighing the elementary powders, blending, stacking and cold compacting followed by pressure-less sintering. The sintering is performed at 1200 °C for 90 min with different cooling rates such as 5 °C/min, 15 °C/min, 20 °C/min and 25 °C/min respectively. In microstructural context, SEM micrographs are the clear evidence for varying microstructure with different percentages of raw materials and cooling rate. Energy dispersive spectroscopy (EDS) technique is used to determine the composition of sintered FGM samples. As a part of mechanical characterization, both green and sintered densities, hardness and flexural strength are evaluated. The results indicate that densities decrease steadily with increased alumina composition and hardness increases with alumina content. The use of PLS15 layer composition with 20 °C/min sinter-cooling rate promoted the best results for the subject FGMs.

Microestructura, dureza y resistencia a la flexión de Ni/Al_2O_3 FGM por sinterización sin presión con diferentes velocidades de enfriamiento

Palabras clave:
Material funcionalmente calificado
Níquel
Alúmina
Metalurgia de polvos
Velocidad de enfriamiento

RESUMEN

En este trabajo, los materiales graduados funcionalmente de cuatro capas (FGM) se fabrican con níquel (Ni) y alúmina (Al_2O_3) como materiales principales. Cuatro FGM de diferentes capas de composición como PLS10, PLS15, PLS20 y PLS25 se preparan a través de pulvimetalurgia. El desarrollo de las FGM de Ni/Al_2O_3 comienza pesando los polvos elementales, mezclando, apilando y compactando en frío, seguido de sinterización sin presión. La sinterización se realiza a 1200 °C durante 90 min con diferentes velocidades de enfriamiento, como

* *Corresponding author.*
E-mail address: ananta.bhaskark@gmail.com (K.A. Bhaskararao).
https://doi.org/10.1016/j.bsecv.2020.03.012

t 5 °C/min, 15 °C/min, 20 °C/min y 25 °C/min, respectivamente. En el contexto microestructural, las micrografías SEM son la evidencia clara de la variación de la microestructura con diferentes porcentajes de materias primas y velocidad de enfriamiento. La técnica de espectroscopia de dispersión de energía (EDS) se utiliza para determinar la composición de muestras de FGM sinterizadas. Como parte de la caracterización mecánica, se evalúan las densidades verdes y sinterizadas, la dureza y la resistencia a la flexión. Los resultados indican que las densidades disminuyen constantemente con una mayor composición de alúmina y la dureza aumenta con el contenido de alúmina. El uso de la composición de la capa PLS15 con una velocidad de enfriamiento de sinterización de 20 °C/min promovió los mejores resultados para las FGM del sujeto.

Introduction

In engineering, all the desired properties cannot be achieved with a single material. Therefore, many engineering components require multi-layered materials in order to successfully satisfy respective design criteria. The components comprising of multi-layered materials may have abrupt interfaces with different in thermal coefficient of expansions. The difference in thermal coefficients between the constituent materials causes cracking, delamination and deterioration of mechanical properties [1]. To circumvent this problem the abrupt interference change is altered with gradient interference by gradually changing the composition of parent materials among the pure materials, this procedure is referred as functionally graded materials (FGMs) [2]. The FGM model has been proposed to increase adhesion and to minimize the thermal stresses in metal-ceramic composites.

FGMs are divided into two broad groups, namely thin FGM and bulk FGM. Thin FGMs are produced by using surface coating techniques like physical/chemical vapour deposition (PVD/CVD) and plasma spraying respectively. Bulk FGMs are fabricated by using methods like centrifugal casting, powder metallurgy, etc. [3,4]. Powder metallurgy is one of the simplest and extensively used methods among the other fabrication techniques to control the composition of the FGMs [5,6]. There are two possible methods to model the FGMs, one is a piecewise variation of volume fraction of elementary materials and the second one is continues variation of volume fraction of the basic materials from one end to the other [7].

Ni/Al_2O_3 blend has drawn significant interest in recent research activities by virtue of its thermo mechanical and physical properties. This combination also exhibits high performance in extreme hot conditions because of its high bonding strength and low residual stress [8]. The Ni/Al_2O_3 FGMs can be designed to take advantage of mechanical properties of metal and heat and corrosion resistance of ceramic without severe internal thermal stresses [9].

Bhattacharyya et al. [10] fabricated the five layered Ni/Al_2O_3 FGM by thermal spray coating. During this investigation, a network type structure with interconnected distribution of α-Al_2O_3 in base matrix was observed. He also reported that the porosity of composite layer depends on size of ceramic particle. Seungkyu et al. [11] studied the dimensional shrinkage of Ni/Al_2O_3 FGM during sintering. He reported that by tailoring the material (layer) composition to provide a uniform shrinkage gradient across the entire sample. Justyna et al. [12] fabricated the hollow cylindrical Ni/Al_2O_3 FGMs by centrifugal casting. Most of the metallic particles were concentrated on the outer surface, whereas the highest concentration of alumina was observed on the inner surface of the sample.

According to the above findings, layer composition, particle size and dispersion of alumina particles is critical for development of FGM. In the present study, layered nickel/alumina (Ni/Al_2O_3) FGMs engineered in different volume fractions is fabricated. The piecewise variation model is chosen in order to fabricate a crack free FGM and powder metallurgy technique is opting for the bulk fabrication. The Al_2O_3 particle dispersion and size variation in Ni matrix of subject FGMs are analysed with different sinter-cooling rates. Hardness and flexural strength of prepared samples also investigated.

Experimental procedure

As received commercially pure Ni powder (Sigma Aldrich, India, >99.7%, 40 μm, spherical shape) and Al_2O_3 (Alfa Aesar, India, >99.7%, 10 μm, irregular shape) were used as raw materials. The size distributions (Fig. 1a and b) of Ni and Al_2O_3 powder particles were recorded using particle size analyser (Olympus, Germany). The Ni/Al_2O_3 bulk FGMs are designed with four layers of variation in the nickel and alumina compositions. Four samples of four layered FGM with different layered composition between Ni and Al_2O_3 were fabricated. The detailed compositional distributions of four layers in the investigating samples are listed in Table 1.

Initially, the required amounts of powder composition were weighed precisely and merged as per the specific volume fractions by considering the size of the specimen and densities of the rudimentary materials. The mixed powders are blended in a high energy planetary ball mill (Fristch GmbH, Germany) for 12 h with a ball to powder ratio of 10:1. The milled powders were warmed up to 150 °C in a vacuum furnace to eliminate the wax from the powders. The powder mixture was stacked layer by layer in high speed steel (HSS) die with an inner diameter of 30 mm as per the composition listed in Table 1. Each layer is shaken and compacted with small loads (<1 ton) before stacking the next layer for attaining homogeneity of compositional distribution throughout the layer. The stacked layers

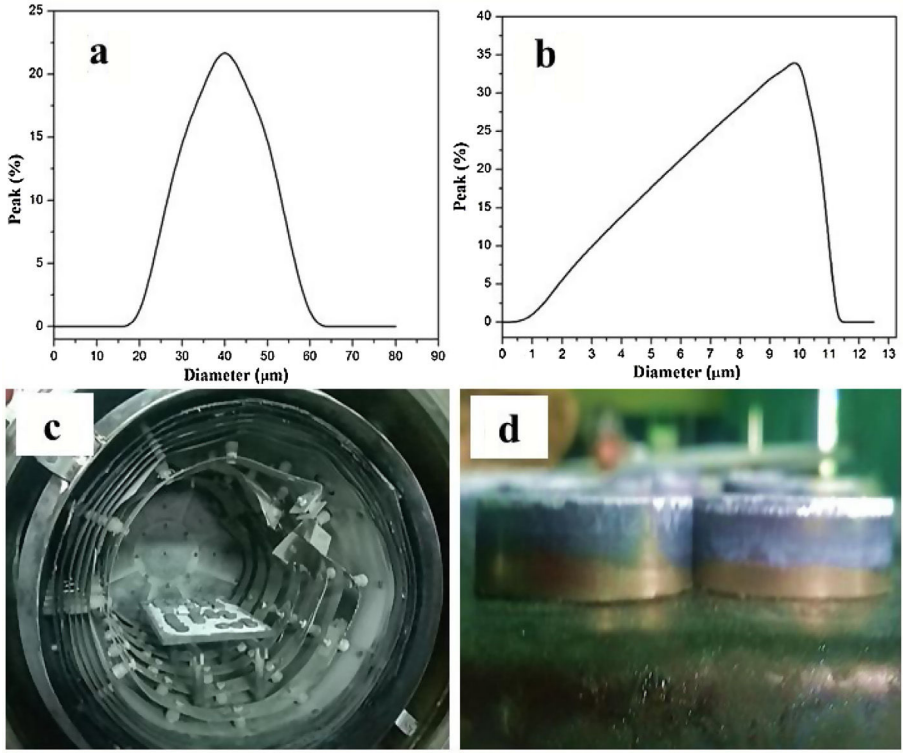

Fig. 1 – Particle size distribution of (a) Ni and (b) Al_2O_3; (c) and (d) consolidated samples.

undergo cold compaction with a load of 20 tons via hydraulic press by uniaxial method.

The green compacts were placed on a graphite plate in order to attain a uniform temperature during the sintering process. The samples were sintered at a temperature of 1200 °C and cooled with different sinter-cooling rates such as 5 °C/min, 15 °C/min, 20 °C/min and 25 °C/min respectively. The sintering time of 90 min was maintained under vacuum atmosphere during the consolidation. The sintered samples of Ni/Al_2O_3 FGMs are shown in Fig. 1c and d. The microstructure of subject FGMs was analysed by a scanning electron microscopy (Hitachi S300N, Japan) equipped with energy dispersive X-ray spectroscopy (EDS) system. The layered microstructure was viewed under back scattered electron image (BSE) mode and secondary electron image (SE) mode at different conditions. The densities of Ni/Al_2O_3 FGMs are estimated in terms of theoretical density. The theoretical density of the composite layers is calculated by hand calcula-

Table 1 – Layered composition of Ni/Al_2O_3 FGMs.

Sample designation	Layer	Elemental composition (wt.%)		Chemical composition (wt.%)
		Ni	Al_2O_3	
PLS10	1	100	–	100% Ni
	2	90	10	90% Ni + 10% Al_2O_3
	3	80	20	80% Ni + 20% Al_2O_3
	4	70	30	70% Ni + 30% Al_2O_3
PLS15	1	100	–	100% Ni
	2	85	15	85% Ni + 15% Al_2O_3
	3	70	30	70% Ni + 30% Al_2O_3
	4	55	45	55% Ni + 45% Al_2O_3
PLS20	1	100	–	100% Ni
	2	80	20	80% Ni + 20% Al_2O_3
	3	60	40	60% Ni + 40% Al_2O_3
	4	40	60	40% Ni + 60% Al_2O_3
PLS25	1	100	–	100% Ni
	2	75	25	75% Ni + 25% Al_2O_3
	3	50	50	50% Ni + 50% Al_2O_3
	4	25	75	25% Ni + 75% Al_2O_3

tions using the rule of mixtures with densities of elementary materials. The green and sintered density of composites was analysed through mass and physical dimensions. The porosity (P) of each composition was expressed in terms of density [13] by the following expression.

$$P = \left[1 - \frac{\rho_S}{\rho_T}\right] \times 100 \quad (1)$$

where P is the porosity of the sample in percentage, ρ_S is the sintered density and ρ_T is the theoretical density. The densities used in the above Eq. (1) are in g/cc.

The hardness of Ni/Al_2O_3 layered composite was evaluated by the Vickers micro hardness tester. The test was performed with a load of 50 g and a dwell time of 15 s in several regions of each layer along the direction of gradation. Three point bending test is conducted to know the flexure strength of the subject FGMs. The pure metal layer is placed at the bottom and the alumina rich composite layer is placed on top in position. The intention behind the arrangement of the specimen is metals have more tensile strength and ceramics have maximum compressive strength.

The flexural test of Ni/Al_2O_3 composites was performed by INSTRON (Model 4201) universal testing machine with 10 kN capacity load cell. The test sample was prepared with a dimension of 40 mm × 11 mm × 11 mm and span distance was 30 mm. The tests were conducted in three point bending mode at a loading rate of 2 mm/min. The average of five sample values of each composition was taken as a final result.

Table 2 – Theoretical and green density of Ni/Al_2O_3 FGMs.

Sample	Theoretical density (g/cc)	Green density (g/cc)
PLS10	8.16	5.04
PLS15	7.75	4.79
PLS20	7.42	4.57
PLS25	7.06	4.34

Results and discussions

Densification studies

Table 2 shows the theoretical and green densities of subject FGMs. The green density of four compositions was around 61.8% of theoretical density. The sintered density and the corresponding porosity values of various compositions of FGMs consolidated at different cooling rates are listed in Tables 3 and 4. The FGMs consolidated at a higher cooling rate (20 °C/min and 25 °C/min) showed higher sintered density as compared to lower cooling rate (5 °C/min and 15 °C/min) sintered FGMs.

As seen in Table 3, the FGMs of PLS15 had exhibited highest sintered density increments, in the range of 3–4%, as compared to the PLS20 and PLS25 FGMs. This may be due to the bonding difference between Ni and Al_2O_3 in layers 3 and 4 of FGMs (Table 1). The increase of ceramic composition in the layers 3 and 4 of PLS20 and PLS25 FGMs could increase the

Table 3 – Sintered density of Ni/Al_2O_3 FGMs.

Samples	Cooling rate – 5 °C/min		Cooling rate – 15 °C/min	
	Sintered density (g/cc)	Relative density (% Th.)	Sintered density (g/cc)	Relative density (% Th.)
PLS10	6.62	81.15	6.88	84.29
PLS15	6.29	81.16	6.53	84.31
PLS20	5.82	78.38	6	80.91
PLS25	5.53	78.32	5.7	80.81
Samples	Cooling rate – 20 °C/min		Cooling rate – 25 °C/min	
	Sintered density (g/cc)	Relative density (% Th.)	Sintered density (g/cc)	Relative density (% Th.)
PLS10	7.11	87.1	7.11	87.11
PLS15	6.75	87.09	6.75	87.1
PLS20	6.2	83.59	6.2	83.6
PLS25	5.9	83.56	5.9	83.57

Table 4 – Porosity of Ni/Al_2O_3 FGMs.

Samples	Cooling rate – 5 °C/min Porosity (%)	Cooling rate – 15 °C/min Porosity (%)	Cooling rate – 20 °C/min Porosity (%)	Cooling rate – 25 °C/min Porosity (%)
PLS10	18.85	15.71	12.90	12.89
PLS15	18.84	15.69	12.91	12.90
PLS20	21.62	19.09	16.41	16.40
PLS25	21.68	19.19	16.44	16.43

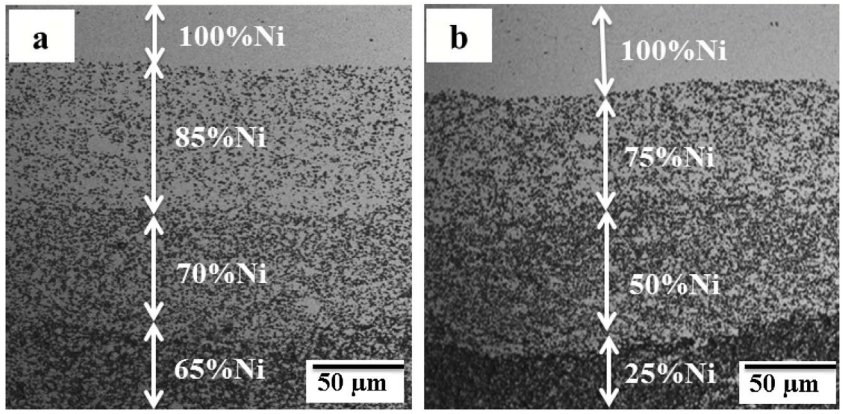

Fig. 2 – BSE micrographs of (a) PLS15 and (b) PLS25 samples.

apparent viscosity of the matrix that enriches the chances of air setup [14]. This is the main reason for an increase in the porosity of PLS20 and PLS25 FGMs. It can be observed that the density variation between PLS10 and PLS15 FGMs is negligible.

Microstructural studies

Fig. 2a and b shows the BSE micrographs of PLS15 and PLS25 FGMs. From the images, four layered structure is perceived. The pure nickel layer is in light phase and the composite layers are seen in gradient dark phase. The microstructure of each layer is different from the adjoining layers and stepwise variation is observed. The bonding of Ni and Al_2O_3 in composite layers is fine and the interfaces of all four layers have appropriate linkages with contiguous layers. The gradient coefficient of thermal expansion is caused for the crack free interference and uniform structures in both sintered FGMs.

The BSE micrographs and the corresponding EDS analysis of layer 3 of PLS15 FGM sintered with different cooling rates are shown in Fig. 3a–h. The EDS analysis of subject FGMs confirmed that the existence of Al_2O_3 (Region + 2) particles in Ni (Region + 1) matrix. The size of alumina grains in numerous regions of sintered layers of PLS15 FGM was estimated from Fig. 3a and e through Image-J software. The calculations were performed from more than 100 particles for each condition. The particle size frequency distribution of FGMs at 5 °C/min and 20 °C/min are shown in Fig. 3d and h. It is observed that cooling rate has a significant effect on the size of Al_2O_3 particles. The microstructure of 20 °C/min sinter-cooled sample showed fine particles of alumina (Fig. 3h) in the Ni matrix. On the other hand, the precipitation of large sized alumina particles (Fig. 3d) was observed in the microstructure of 5 °C/min sinter-cooled sample. Similar observations were made in the microstructure of PLS25 FGM sintered under the cooling rate of 5 °C/min and 20 °C/min (Fig. 4a–h).

Table 5 shows the average size of alumina particles in numerous regions of sintered layers of subject FGMs. It can be noted that there is a large deviation with the size of alumina particles in the respective layers of PLS15 and PLS25 samples. The average size of alumina particles in layer 4 of PLS15 FGM at 20 °C/min is 11.6 µm. However, the value increased to 21.6 µm in layer 4 of PLS25 FGM for the same condition. This is due to the difference in the elemental concentration of Al_2O_3 particles in the layer 4 of PLS15 and PLS25 FGMs. The large concentration (75%) of Al_2O_3 in layer 4 of PLS25 caused the formation of coarse sized Al_2O_3 particles. Increasing ceramic particle concentration in the base matrix can apparently increase the final size of the reinforced particle [15].

Fig. 5a–d shows the SEM micrographs in layer 4 of PLS15 and PLS25 FGMs sintered with a cooling rate of 5 °C/min and 20 °C/min respectively. The PLS15 FGM sintered at a cooling rate of 5 °C/min (Fig. 5a) had large sized pores. On the other hand, the 20 °C/min sinter-cooled FGM (Fig. 5a) had small sized pores. This indicates that the pore size reduced as the sinter-cooling rate increased. On the contrary, PLS25 FGM at a higher cooling rate (20 °C/min) had large sized pores (Fig. 5d). This is because of the variation in the layered composition between PLS15 and PLS25 FGMs. The high concentration of Al_2O_3 (Table 1) and precipitation of coarse sized particles (Table 5) in PLS25 FGM may increase the size of pores [16].

Hardness

The hardness results of different layers of subject FGMs at different cooling rates are shown in Fig. 6 and the corresponding values are listed in Table 6. The average of eight values taken from different regions of each layer is considered for the final results. As seen in Fig. 6, the hardness of pure nickel layer (1) of subject FGMs is in the range of 128–130 HV. The variation in hardness is observed from pure nickel layer to composite layers of subject FGMs. It can be found that the hardness increases fast with the increase of Al_2O_3 concentration in the respective layers. When increasing the concentration of Al_2O_3 from 0% (layer 1) to 45% (layer4), the hardness increments of PLS15 FGM are in the range of 32–36% (Table 6).

In the case of PLS25 sample, when increasing the alumina content from 0% (layer 1) to 75% (layer 4), the hardness increments is in the range of 28–32%. The reason for this variation is due to the difference in porosity values as observed in the samples (Table 4). The sample of PLS15 got less porosity when compared to the sample of PLS25. Because of this reason, PLS15 composite layers reported higher hardness when compared to PLS25 composite layers. As seen in Fig. 6a–d, the hardness of layer 4 of PLS15 FGM sinter-cooled by 20 °C/min is

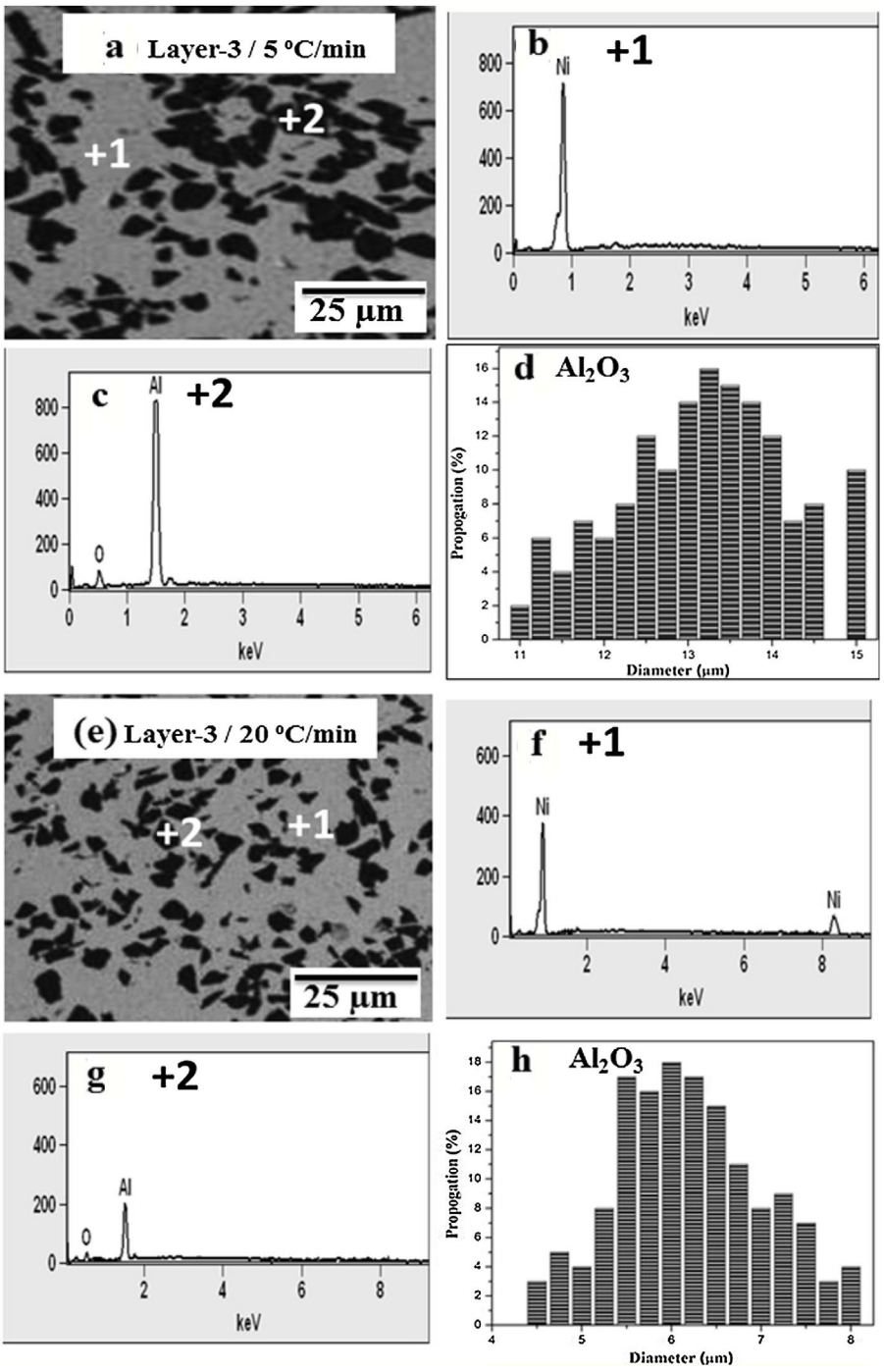

Fig. 3 – BSE micrographs and EDS analysis of PLS15 samples: consolidated at (a)–(d) 5 °C/min; (e)–(h) 20 °C/min.

205 HV, which is higher than the 5 °C/min sinter-cooled FGM with a hardness of 188 HV.

Flexural strength

The stress–strain curves of subject FGMs consolidated at different cooling rates are shown in Fig. 7 and the corresponding flexural strength values are listed in Table 7. The PLS15 FGMs sinter-cooled by 20 °C/min underwent 6% plastic deformation prior to fracture and flexural strength is 140 MPa. This value is significantly higher than the PLS25 sample of the same condition with a flexural strength of 126 MPa. The high strength of PLS15 sample is primarily attributed to less porosity (Fig. 5b) as well as high hardness (Fig. 6c) observed after sintering.

It is also noted that better flexural strength seems to be exhibited by higher cooling rate (20 °C/min and 25 °C/min) sintered samples compared to lower cooling rate (5 °C/min and 15 °C/min) sintered samples. This is due to homogenous dispersion of fine grained ceramic particles in the base matrix (Figs. 3e and 4e) as obtained with higher sinter-cooling rates.

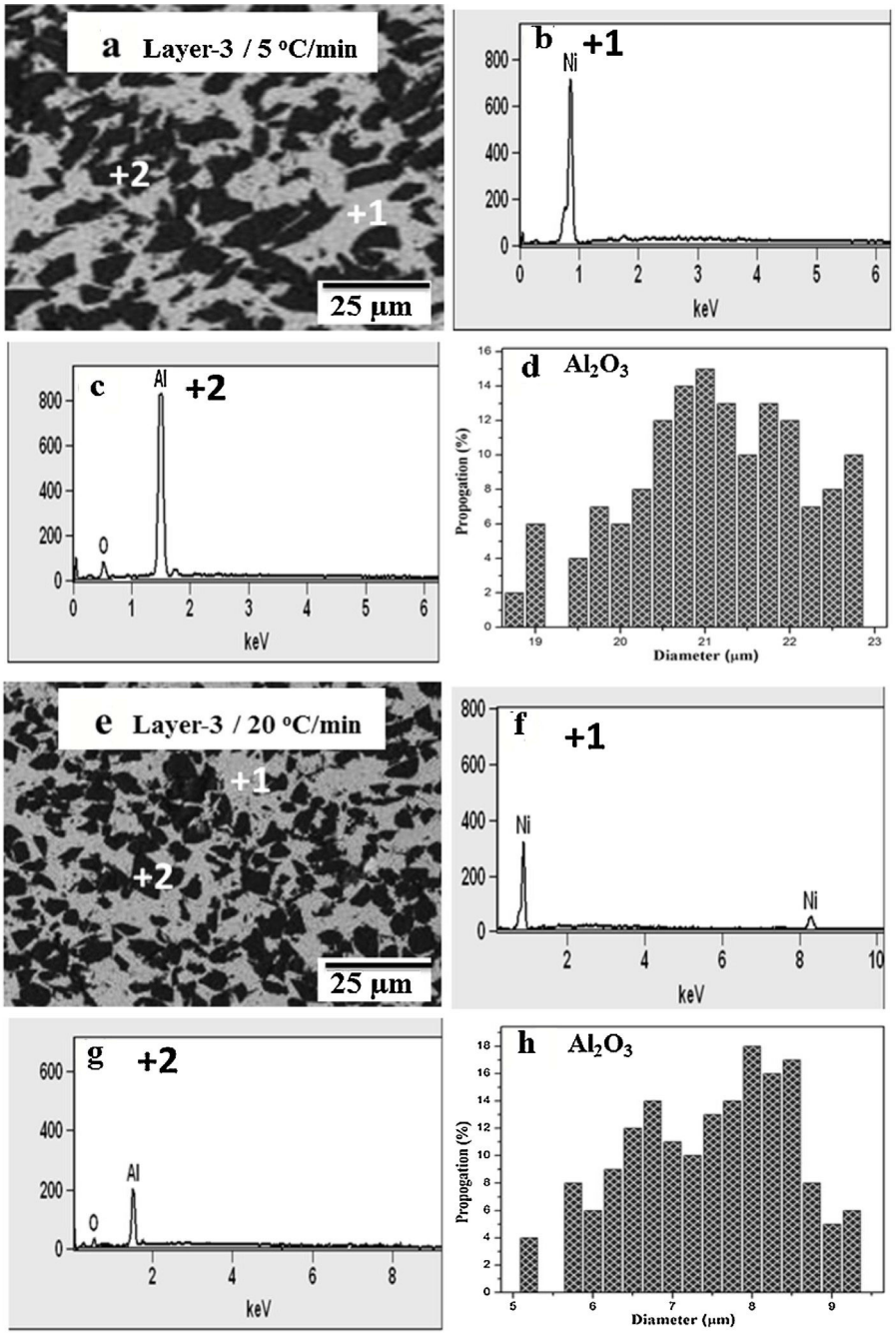

Fig. 4 – BSE micrographs and EDS analysis of PLS25 samples: consolidated at (a)–(d) 5 °C/min; (e)–(h) 20 °C/min.

Table 5 – Average size of alumina particles in Ni/Al_2O_3 composite layers.

Sample	Cooling rate (°C/min)	Layer 2 Particle size (µm)	Layer 3 Particle size (µm)	Layer 4 Particle size (µm)	Average particle size (µm)
PLS15	5	6.72	13.57	22.48	14.26
	15	5.93	9.52	16.72	10.72
	20	4.65	6.84	11.59	7.69
	25	4.61	6.80	11.54	7.65
PLS25	5	9.58	21.63	38.38	23.20
	15	8.39	14.74	30.64	17.92
	20	7.74	8.56	21.63	12.64
	25	7.71	8.53	21.61	12.61

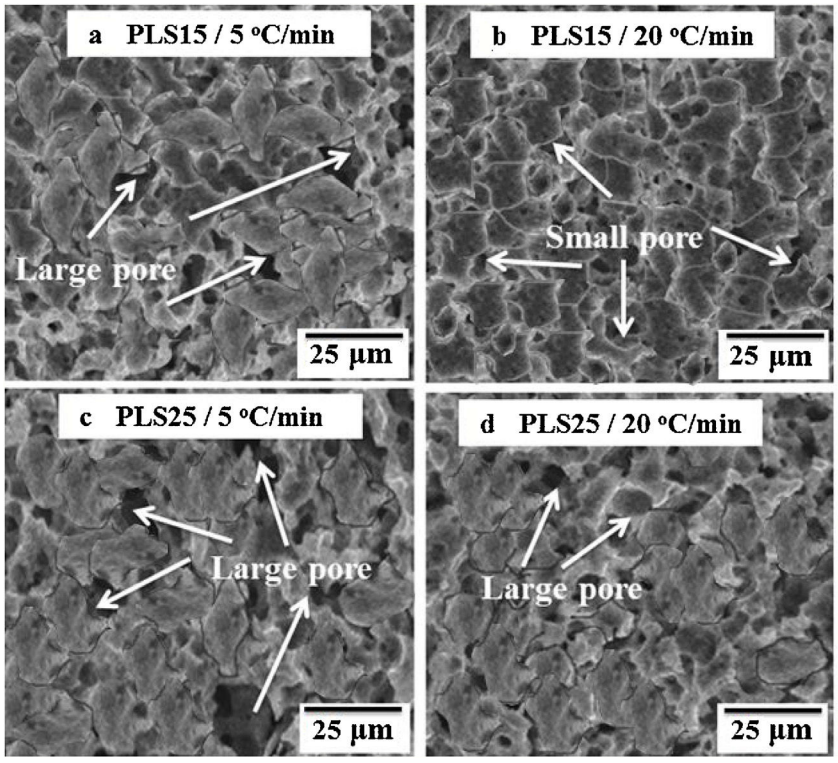

Fig. 5 – SEM micrographs of Ni/Al_2O_3 FGMs: PLS15 at (a) 5 °C/min and (b) 20 °C/min; PLS25 at (c) 5 °C/min and (d) 20 °C/min.

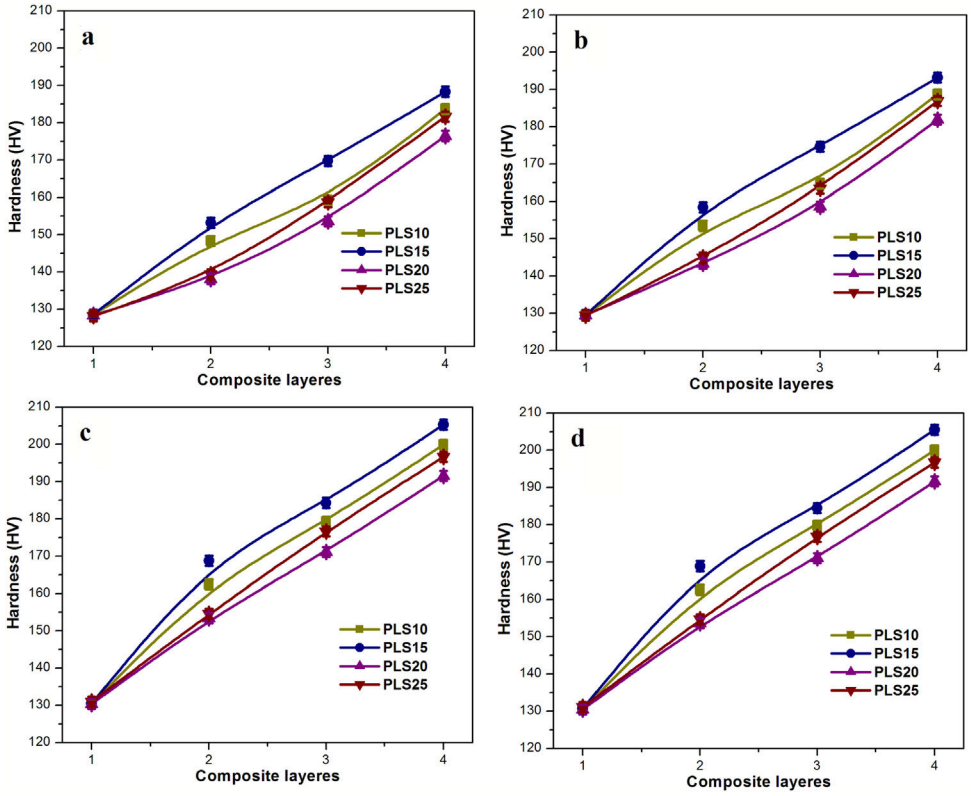

Fig. 6 – Hardness of FGMs consolidated at different cooling rates: (a) 5 °C/min; (b) 15 °C/min; (c) 20 °C/min; (d) 25 °C/min.

Table 6 – Hardness values of Ni/Al_2O_3 composite layers.

Sample	Layer	Cooling rate – 5 °C/min Hardness (HV)	Cooling rate – 15 °C/min Hardness (HV)	Cooling rate – 20 °C/min Hardness (HV)	Cooling rate – 25 °C/min Hardness (HV)
PLS10	1	128 ± 1	129 ± 1.5	130 ± 1	130 ± 1
	2	148 ± 1.5	153 ± 1.5	162 ± 1	163 ± 1
	3	159 ± 2	165 ± 2	179 ± 2	180 ± 2
	4	184 ± 2	189 ± 2	200 ± 2	200 ± 2
PLS15	1	129 ± 1	129 ± 1	130 ± 1	130 ± 1
	2	153 ± 2	158 ± 1	169 ± 1	169 ± 1
	3	169 ± 1.5	174 ± 2	184 ± 1.5	184 ± 1.5
	4	188 ± 2	193 ± 2	205 ± 1.5	205 ± 1.5
PLS20	1	128 ± 1.5	129 ± 1.5	130 ± 1	130 ± 1
	2	138 ± 2	143 ± 2	153 ± 2	154 ± 1.5
	3	154 ± 2.5	159 ± 2	171 ± 2.5	171 ± 2.5
	4	176 ± 2.5	182 ± 2.5	191 ± 2	192 ± 1.5
PLS25	1	128 ± 1	129 ± 1	130 ± 1	130 ± 1
	2	139 ± 2.5	145 ± 2.5	155 ± 2.5	155 ± 2
	3	159 ± 2.5	163 ± 2.5	177 ± 2.5	177 ± 2
	4	181 ± 2.5	187 ± 2	197 ± 2.5	197 ± 2

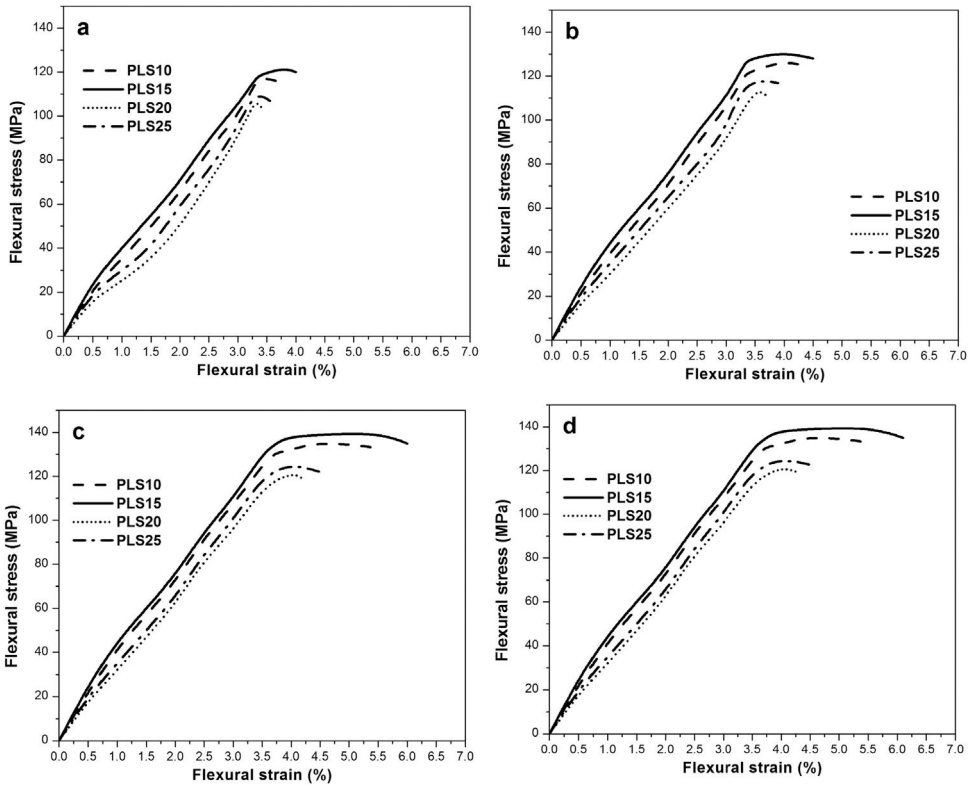

Fig. 7 – Stress–strain curves of FGMs consolidated at different cooling rates: (a) 5 °C/min; (b) 15 °C/min; (c) 20 °C/min; (d) 25 °C/min.

Table 7 – Flexural strength values of Ni/Al_2O_3 composites.

Sample	Cooling rate – 5 °C/min Flexural strength (MPa)	Cooling rate – 15 °C/min Flexural strength (MPa)	Cooling rate – 20 °C/min Flexural strength (MPa)	Cooling rate – 25 °C/min Flexural strength (MPa)
PLS10	119 ± 8	128 ± 12	136 ± 12	136 ± 12
PLS15	122 ± 9	131 ± 13	140 ± 12	140 ± 12
PLS20	108 ± 9	115 ± 12	123 ± 11	123 ± 11
PLS25	112 ± 8	120 ± 12	126 ± 11	127 ± 11

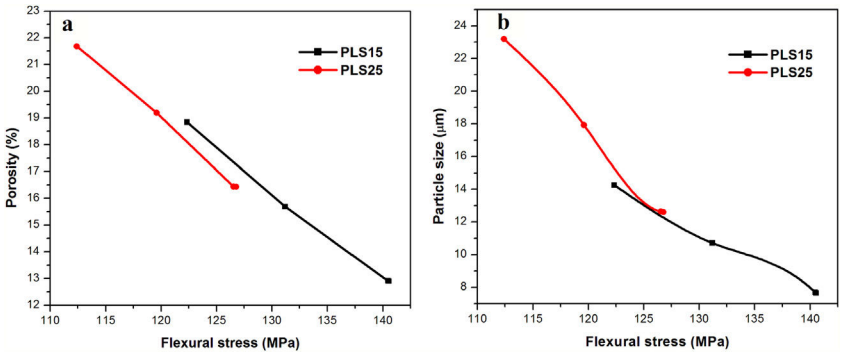

Fig. 8 – Variation of flexural strength with (a) porosity and (b) particle size.

Moreover, the reduced levels of porosity at a sinter-cooling rate of 20 °C/min and 25 °C/min (Table 4) also contribute towards improvement in the strength of the samples. It is to be noted that the flexural strength increases with an increase in the hardness of subject FGMs.

Variation in the flexural strength with respect to the porosity and the particle size of subject FGMs are shown in Fig. 8a and b. It can be seen that the strength increase with the decrease in porosity and particle size. The less porosity (12%) and smallest alumina particle of size 7.6 μm obtained for PLS15 FGM sinter-cooled at 20 °C/min registered the higher flexural strength values.

Discussion on the effect of cooling rate in composite layers

It is worth noting that the sintered density of Ni/Al_2O_3 FGMs increases with increase in cooling rate during pressure less sintering. It is considered due to particle size variation in respective composite layers. The small size particles as formed at higher cooling rates (Table 5) have large mass transportation that eliminates the porosity [17].

Microstructure of Ni/Al_2O_3 FGMs was studied as a function of cooling rate used during pressure-less sintering. The degree of precipitation is low for the FGMs sintered with the higher cooling rate (Fig. 3e) as compared to lower cooling rate (Fig. 3a). FGMs of all compositions consolidated by 5 °C/min showed high quantity large sized alumina particles in the Ni matrix. On the other hand, less quantity of small sized alumina particles is presented the Ni matrix of 20 °C/min sinter-cooled FGMs. This is a reasonable observation because the time for precipitation of coarse sized ceramic particles is low at higher sinter-cooling rates [18,19].

It is deduced that 5 °C/min sinter-cooled samples of all compositions show lesser hardness. The decrement on the hardness values can be based on uneven distribution of large sized ceramic particles (Figs. 3a and 4a) in the base matrix. These high quantities large particles may deteriorate the precipitation strengthening which could lead to poor interface between reinforced particle and base matrix [20]. This is the main reason for early deformation as observed in lower sinter-cooled FGMs (Fig. 7). Nevertheless, higher sinter-cooling rate with 20 °C/min exhibited better bending properties. This is due to uniform distribution of ceramic particles in the base matrix and thus weakens the stress concentration at the interface [21].

Regarding experimental factors, it is worthwhile to notice that the sinter-cooling rate and layered composition played a relevant role to define the mechanical properties of Ni/Al_2O_3 FGMs. The results reveal that the density, hardness and strength of FGMs significantly improved by increase of cooling rate, but when cooling rate is above 20 °C/min, the properties increases slowly. It can be pointed out that the density (Tables 2 and 3) and porosity (Table 4) variation between PLS10 and PLS15 FGMs and also between PLS20 and PLS25 FGMs are negligible.

Conclusions

A four-layered Ni/Al_2O_3 FGM samples are obtained by a simple method of cold compacting and pressure-less sintering with different sinter-cooling rates. Four samples of PLS10, PLS15, PLS20 and PLS25 with different compositional gradients are prepared. From the micrographs, the variation in microstructures with respect to composite layer is noticed. The compositional elements of subject FGMs are confirmed with the EDS technique and no other material is found except constituent materials in all layers.

In this work we demonstrated that

- The increase in the porosity of PLS20 and PLS25 composite layers is observed. It has been suggested that the increase of Al_2O_3 concentration in composite layers leads to decrease of the final density of the sample.
- Microstructural studies proved that the layer composition with sinter-cooling rate has a significant effect on the degree of precipitation and ceramic particle size.
- Hardness test revealed that the hardness of PLS15 composition with 20 °C/min fast-cooled FGM is more pronounced than the hardness recorded at all other conditions. The reduction in porosity and even dispersion of fine particles of Al_2O_3 was the cause for this expected behaviour.
- One can note that hardness increases with increase of Al_2O_3 concentration in the respective layers of subject FGMs.
- Hardness results are correlated with bending properties of subject FGMs.

In the view of the above findings, Ni/Al_2O_3 FGM of PLS15 layered composition fabricated by pressure less sintering with a cooling rate of 20 °C/min appears to exhibit possible formation of microstructure and better mechanical properties.

Acknowledgement

The authors would like to express their gratitude to Jawaharlal Nehru Technological University, India for motivating to publish the research paper. The experiments and analysis in the present study were carried out in International Advanced Research Centre for Powder Metallurgy and New Materials (ARCI), India.

REFERENCES

[1] Y. Miyamoto, W.A. Kaysser, B.H. Rabin, A. Kawasaki, R.G. Ford, Functionally Graded Materials: Design, Processing and Applications, Springer US, 1999.
[2] A.V. Shevchenko, et al., Functional graded materials based on ZrO_2 and Al_2O_3 production methods, Powder Metallur. Met. Ceram. 42 (2003) 145–153.
[3] J. Jerzy, L. Drenchev, J. Jerzy, L. Drenchev, Metallic functionally graded materials: a specific class of advanced composites, J. Mater. Sci. Technol. 29 (4) (2013) 297–316.
[4] Y. Watanabe, Y. Hattori, H. Sato, Distribution of microstructure and cooling rate in Al–Al_2Cu functionally graded materials fabricated by a centrifugal method, J. Mater. Process. Technol. 221 (2015) 197–204.
[5] P.K. Kumar, N.V. Sai, A.G. Krishna, Influence of sintering conditions on microstructure and mechanical properties of alloy 218 steels by powder metallurgy route, Arab. J. Sci. Eng. 10 (2018) 116–121.
[6] E. Restrepo, et al., Influencia de los esfuerzos residuales en la adherencia de recubrimientos de Al_2O_3–40% TiO_2 depositados mediante proyección térmica por combustión, Bol. Soc. Españ. Cerám. Vid. 55 (2016) 219–227.
[7] F. Ebrahimi, Advances in Functionally Graded Materials and Structures, Intech Open Access Publisher, Croatia, 2016.
[8] T.T. Dele-Afolabi, et al., Significant effect of rice husk and sugarcane bagasse pore formers on the microstructure and mechanical properties of porous Al_2O_3/Ni composites, J. Alloys Comp. 743 (2018) 323–331.
[9] D. Gayen, R. Tiwari, D. Chakraborty, Static and dynamic analyses of cracked functionally graded structural components: a review, Compos. Part B: Eng. 173 (2019).
[10] M. Bhattacharyya, A.N. Kumar, S. Kapuria, Synthesis and characterization of Al/SiC and Ni/Al_2O_3 functionally graded materials, Mater. Sci. Eng. A 487 (2008) 524–535.
[11] Y. Seungkyu, H. Kim, C.S. Lee, Investigation of shrinkage control in Ni–Al_2O_3 (metal–ceramic) functionally graded materials, Ceram. Int. 39 (2013) 93–99.
[12] Z. Justyna, P. Wiecińska, A. Miazga, et al., Al_2O_3/Ni functionally graded materials (FGM) obtained by centrifugal-slip casting method, J. Therm. Anal. Calorim. 130 (2017) 123.
[13] G.W. Horgan, An investigation of the geometric influences on pore space diffusion, Geoderma 88 (1999) 55–71.
[14] M. Aminzare, Reaction-bond sintering of C/SiC functionally graded nanostructured materials (FGNMs), Mater. Sci. Eng. A 565 (2013) 445–449.
[15] Kumar, Vijaya, Gopala, N. Renganathan, Fabrication and micro-structural evaluation of ODS austenitic stainless steels through mechanical alloying, Mater. Today Proc. (2019).
[16] R. Narayanasamy, T. Ramesh, M. Prabhakar, Effect of particle size of SiC in aluminium matrix on workability and strain hardening behaviour of P/M composite, Mater. Sci. Eng. A 504 (2009) 13–23.
[17] P.K. Kumar, et al., Effect of Y_2O_3 and ZrO_2 on the microstructure and mechanical properties of Nano-ODS 21Cr–9Mn–6Ni steels, Mater. Technol. 52 (4) (2018) 493–497.
[18] M. Madhan, G. Prabhakaran, Microwave versus conventional sintering: microstructure and mechanical properties of Al_2O_3–SiC ceramic composites, Bol. Soc. Españ. Cerám. Vid. 58 (2019).
[19] K. Kumar, et al., Effect of Y_2O_3 addition and cooling rate on mechanical properties of Fe–24Cr–20Ni–2Mn steels by powder metallurgy route, Compos. Commun. 10 (2018) 116–121.
[20] M. Shabani, R. Paydar, Zamiri, et al., Microstructural and sliding wear behavior of SiC-particle reinforced copper matrix composites fabricated by sintering and sinter-forging processes, J. Mater. Res. Technol. 5 (2016) 5–12.
[21] N. Radhika, R. Raghu, Development of functionally graded aluminium composites using centrifugal casting and influence of reinforcements on mechanical and wear properties, Trans. Nonferrous Met. Soc. China 26 (2016) 905–916.